A novel poly(vinyl carbonate-co-butyl acrylate) quasi-solid-state electrolyte as a strong catcher for lithium polysulfide in Li–S batteries

A novel poly(vinyl carbonate-co-butyl acrylate) quasi-solid-state electrolyte as a strong catcher for lithium polysulfide in Li—S batteries

Bei Ye[a1], Xiaomin Cai[a1], Dongya Wang[a], Petr Saha[b], Gengchao Wang[a] *

[a]*Shanghai Key Laboratory of Advanced Polymeric Materials, Shanghai Engineering Research Center of Hierarchical Nanomaterials, School of Materials Science and Engineering, East China University of Science and Technology, Shanghai, 200237, China*

[b]*Centre of Polymer Systems, University Institute, Tomas Bata University Tr. T Bati 5678, Zlin, 76001, Zlín, Czech Republic*

ABSTRACT

Lithium-sulfur batteries show great potential in the field of energy storage because of their high-energy density, but the shuttle effect of lithium polysulfide has seriously hindered their practical process. Quasisolid-state electrolyte (QPE) is considered to be a promising alternative to traditional liquid electrolyte, which can improve the safety and cycling performance of lithium-sulfur batteries. Herein, a novel poly(vinyl carbonate-co-butyl acrylate) QPE with 3D crosslinked network (PEGDA-P(VCA-co-BA)) is designed to capture lithium polysulfide through a chemical adsorption of abundant ester groups. The PEGDA-P(VCA-co-BA) QPE exhibits high ionic conductivity of 2.9 mS cm^{-1}. In order to synergize the beneficial effect of the PEGDA-P(VCA-co-BA) QPE, the nitrogen-doped carbon nanotube film-supported sulfur/Li cells are assembled with the QPE. As-assembled lithium-sulfur batteries show high initial capacity of 1080 mAh g^{-1} at 0.1 C, long cycle life (capacity retention of 715 mAh g^{-1} after 500 cycles) and superior rate performance.

Keywords: Quasi-solid-state polymer electrolytes, cross-linked, flexible cathode, lithium-sulfur batteries

1. Introduction

With the rapid development of new energy vehicles and consumer electronics, traditional lithium-ion batteries are difficult to meet the requirements of high-energy density [**1,2**]. The theoretical energy density of lithium-sulfur batteries can reach 2600 Wh kg^{-1}, which is 3—5 times higher than that of traditional lithium-ion batteries [**3,4**]. In addition, the positive active substance, sulfur, is cheap and environmentally friendly [**5**]. Therefore, Li—S batteries are recognized as the most promising secondary battery system for the next-generation [**6**]. However, the low conductivity of elemental sulfur and lithium sulfide discharged products, serious volume deformation during charging and discharging, shuttle effect of lithium polysulfides (LiPSs) and lithium dendrites of the anode greatly reduce the utilization of active materials and cycle life of Li—S batteries, which seriously hinders the practical process of Li—S batteries [**7,8**].

Electrolyte is the medium of lithium-ion fast transmission between cathode and anode [**9**]. Its properties directly affect the charging and discharging behavior of active substances in batteries [**10**]. Traditional liquid electrolytes not only accelerate sulfur shuttle, but also have the risk of leakage and combustion. Quasisolid-state polymer electrolyte (QPE) has the advantages of both liquid electrolyte and all-solid electrolyte [**11**]. It can not only physically isolate cathode and anode, but also has high room temperature ionic conductivity (compared with most all-solid-state polymer electrolytes), low interface impedance and good mechanical strength [**11,12**].

There is a lithium bond between electron donor group and LiPSs, so it can provide effective binding sites for LiPSs, and this binding is independent of surface area, but related with the volume density of the electron donor group [**13,14**].Polyvinylidene carbonate (PVCA) contains carbonate bonds with high spatial density, which can bind lithium polysulfide more effectively [**15,16**]. However, its intrinsic brittleness will lead to interface contact problems with lithium metal, which seriously limits its practical application [**17**]. Some studies have shown that the rigid-flexible network structure improves the ionic conductivity of QPE [**18**]. Therefore, a flexible segment butyl acrylate (BA) can be introduced through this concept [19,20]. On the one hand, abundant ester groups can capture lithium polysulfide and form an optimized SEI film on the lithium anode [**21,22**]. On the other hand, the movement of flexible segments can accelerate the migration of lithium ions and effectively improve the ionic conductivity of QPE [**23,24**].

In addition, because of the insulating property of sulfur, it cannot be used as cathode material alone, but must be combined with conductive materials [**25,26**]. At present, various kinds of carbon materials, such as graphene [**27—29**], carbon nanotubes [**30—32**], porous carbon [**33—35**] and so on, are mainly used to compound with sulfur. However, the affinity between non-polar carbon surface and polar LiPSs is very poor [**36**]. Carbon materials can only play a physical adsorption role, and cannot fundamentally solve the problem of sulfur shuttle. Some studies have shown that carbon materials doped with monoatomic nitrogen have strong adsorption on LiPSs [**31,34,36,37**]. This is attributed to the fact that N atom with additional electron pairs can act as Lewis sites to form chemical bonds with Li+ in LiPSs, thus inhibiting the dissolution of LiPSs to a certain extent [**38**].

Herein, we prepared a new type of QPE, which solved the brittleness of PVCAby free radical copolymerization of VCA and flexible monomer BA. The addition of macromolecular cross-linked agent (poly(ethylene glycol) diacrylate, PEGDA) improves the solvent resistance of QPE. In addition, carbon nanotubes were used as conductive substrates and polypyrrole (PPy) as nitrogen source to realize pyridine nitrogen and pyrrole nitrogen doping with stronger adsorption effect. The double adsorption of LiPSs by the QPE with rich ester groups and the nitrogen-doped cathode successfully improved the rate performance and cycle stability of the Li—S battery. As a result, the initial discharge capacity of the assembled Li—S battery is 1080 mAh g^{-1} (675 mAh g^{-1} of the entire cathode) at 0.1 C. After 500 long cycles, the specific capacity of the battery is still 715 mAh g^{-1}, with an average capacity attenuation of only 0.068% per cycle. Even at a high rate of 2 C, the battery still has a considerable capacity of 628 mAh g^{-1}.

2. Experimental section

2.1. Preparation of PEGDA-P(VCA-co-BA)/LiTFSI-DOL/DME quasisolid-state polymer electrolyte

Firstly, vinylene carbonate (VCA) and butyl acrylate (BA) monomers with a certain mole ratio were added to a 50 mL flask, followed by 5 wt% benzoyl peroxide (BPO) initiator. After stirring at 80° C for a period of time, the flask was quickly cooled to room temperature. Subsequently, a certain mass of poly(ethylene glycol) diacrylate (PEGDA) macromolecular cross-linked agent was added. After being uniformly stirred under 60° C, the viscous liquid was injected into the glass plate mold and the mold was placed in an oven at 80 ° C for 6 h, and then heated to 100° C for 2 h to obtain PEGDA-P(VCA-co-BA) copolymer films. The as-prepared PEGDA-P(VCA-co-BA) films were extracted with acetone to remove unreacted monomers, which were then placed in a vacuum oven and dried at 60° C for 24 h to constant weight. After that, the films were transferred to a glove box and immersed in 1 M lithium bis(trifluoromethane) sulfonamide (LiTFSI) in a binary solvent of dimethoxymethane/1,3-dioxolane (DME/DOL, 1:1 by volume) solution. Finally, the PEGDA-P(VCA-co-BA/LiTFSI—DOL/DME quasisolid-state polymer electrolytes (QPE) were obtained. The exact amounts of reagents were listed in **Tables S1 and S2**.

2.2. Preparation of N(PPy)-CNT@S self-standing cathode

Firstly, carbon nanotube (CNT) films (Suzhou Jedi Nanotechnology Co., Ltd., China) were treated in ethanol by ultrasound for 10 h at room temperature, and then the expanded carbon nanotube films were obtained. Using polypyrrole (PPy) as nitrogen source, CNT@PPy was prepared by electro-polymerization in aqueous solution containing 0.02 M KCl, 0.001 M HCl, and 0.05 M pyrrole. CNTs were used as the working electrode, Pt was used as the counter electrode, and saturated calomel as the reference electrode. CNT@PPy composite films with different PPy contents were prepared by potentiostatic polymerization (0.7 V) with controlled charge amounts of 1.5 C, 3.6 C and 7.2 C, respectively. Composite films were obtained by freeze-drying (pre-freezing for 2 h and then sublimation drying for 24 h) after repeated washing with deionized water and ethanol. Nitrogen-doped CNTs (N(PPy)-CNT) were obtained by carbonizing the product in a tubular furnace at a rate of 2°C min-1 to 800°C, holding for 2 h and cooling naturally to room temperature.

Subsequently, N(PPy)-CNT was immersed in 0.2 M Na2S solution, platinum sheet was used as reference electrode and opposite electrode, and sulfur ion was oxidized to sulfur element on N(PPy)-CNT electrode by potentiostatic method. The potential was 1.25 V and the charge was 15 C. After that, the residual ions in the solution were removed by repeated washing with deionized water, and N(PPy)-CNT@S was obtained by freeze-drying. In order to increase the contact between sulfur and CNTs, the product was treated in a hydrothermal reactor at 155°C for 12 h, and then dried in vacuum at 60°C for 24 h to obtain N(PPy)-CNT@S self-standing cathode.

2.3. Characterizations and instruments

Morphologies of the samples were characterized by field emission scanning electron microscopy (FE-SEM,Hitachi S-4800). The elemental mapping analysis was carried out by using an energy dispersive spectrometer (EDS, QUANTAX 400—30). X-ray diffraction (XRD) was conducted using a Rigaku D/Max 2550 VB/PC X equipped with a Cu target X-ray tube between 5° and 75°. Raman spectra were obtained using a Renishaw Via Reflex Raman scattering microscope with a wavelength of 514 nm. Thermogravimetric (TG) analysis was measured on a TG instrument (STA409PC) at a heating rate of 10

°C min^{-1} under N_2 atmosphere. Attenuated Total Reflection-Fourier transform infrared spectroscopy (ATR-FTIR) spectra were collected using a Nicolet 6700 spectrometer equipped with a Smart OMNI Sampler. X-ray photoelectron spectroscopy (XPS, ESCALAB 250Xi, Thermo Scientific) with Al Ka X-ray source was performed. The mechanical properties of the PEGDA-P(VCA-co-BA) membranes were measured on a Zwick Roell universal testing machine at a stretching speed of 10 mm min^{-1}.

The electrolyte uptake amount of the membrane was tested by immersing the as-prepared membrane into the liquid electrolyte for a certain time. Subsequently, the excess solution on the surface of the membrane was slightly absorbed by the filter paper. The electrolyte uptake ratio (EUR) was calculated by the following equation: EUR (%) = (W_a - W_b) x 100/W_b, where W_a and W_b represented the weight of membrane after and before immersion, respectively.

The ionic conductivity (s) of the polymer electrolytes was measured by AC impedance spectroscopy using a CHI 760 C electrochemical workstation in the frequency range from 100 kHz to 0.01 Hz with an AC amplitude of 5 mV. And the value can be estimated by the equation s = l/(R_b x A), where l is the thickness (cm) of the membrane, R_b is the bulk resistance (u) obtained from the first intercept on the c-axis of the impedance figures, and A is the contact area (cm^2) of the membrane with the current collector.

2.4. Cells assemble and electrochemical measurements

The lithium-ion transference number (t_{Li+}) of electrolyte was calculated by Bruce-Vincent-Evans equation [**39**]:

$$t_{Li^+} = \frac{I_{ss}}{I_o} \cdot \frac{V - I_o R_o}{V - I_{ss} R_{ss}}$$

Where I_o is the initial polarization current, and I_{ss} is the steady-state current of Li//Li symmetrical battery under the applied polarization voltage of 10 mV. R_o and R_{ss} are the initial interfacial resistance and the steady-state interfacial resistance after polarization, respectively.

The 0.05 M Li_2S_6 solution was prepared by dissolving elemental S and Li2S in a molar ratio of 5:1 in DME/DOL (v/v = 1:1) at 65°C with vigorous stirring for 24 h.

The coin cells were assembled by using N(PPy)-CNT@S as cathode, PEGDA-P(VCA-co-BA) as QPE, and lithium sheet as anode in Ar-filled glove box. The electrolyte contains 1 M lithium bis(tri-fluoromethane) sulfonamide (LiTFSI) in a binary solvent of dime-thoxymethane/1,3-dioxolane (DME/DOL, 1:1 by volume) with 1 wt % $LiNO_3$ as additive. For comparison, the N(PPy)-CNT@S/PP/Li cells were assembled in the same way except using polypropylene (PP) separator (celgard 2400) instead of QPE. The Galvano static charge/ discharge test was carried out on a LAND CT2001A battery tester between 1.7 and 3.0 V (versus Li/Li^+). The electrochemical impedance spectra (EIS) (frequency range: 0.01—100 kHz; amplitude: 5 mV) were conducted on a CHI 760E electrochemical workstation.

3. Results and discussion

In order to improve the solvent resistance of P(VCA-co-BA) copolymers, we introduced the macromolecular cross-linked agent PEGDA. **Fig. S1** illustrated the necessity of introducing PEGDA. The 3D crosslinked PEGDA-P(VCA-co-BA) QPE were synthesized by radical polymerization as shown in **Fig. 1**a. VCA and BA monomers were polymerized under BPO initiator, and the addition of macromolecular

cross-linked agent (PEGDA) formed a 3D cross-linked structure. As shown **Fig. 1**b, the FTIR spectra exhibit the absorption peaks at 1635 cm-1,1637 cm-1 and 1630 cm^{-1} corresponding to the C=C stretching vibration of VCA, BA and PEGDA, respectively. It is noteworthy that in the PEGDA-P(VCA-co-BA) copolymer, the C=C characteristic peak disappeared, which proved the polymerization of above monomers. In addition, the absorption peaks at 1825 cm^{-1} and 1725 cm^{-1} of the PEGDA-P(VCA-co-BA) are attributed to the carbonate groups of VCA and the ester group of BA, respectively.

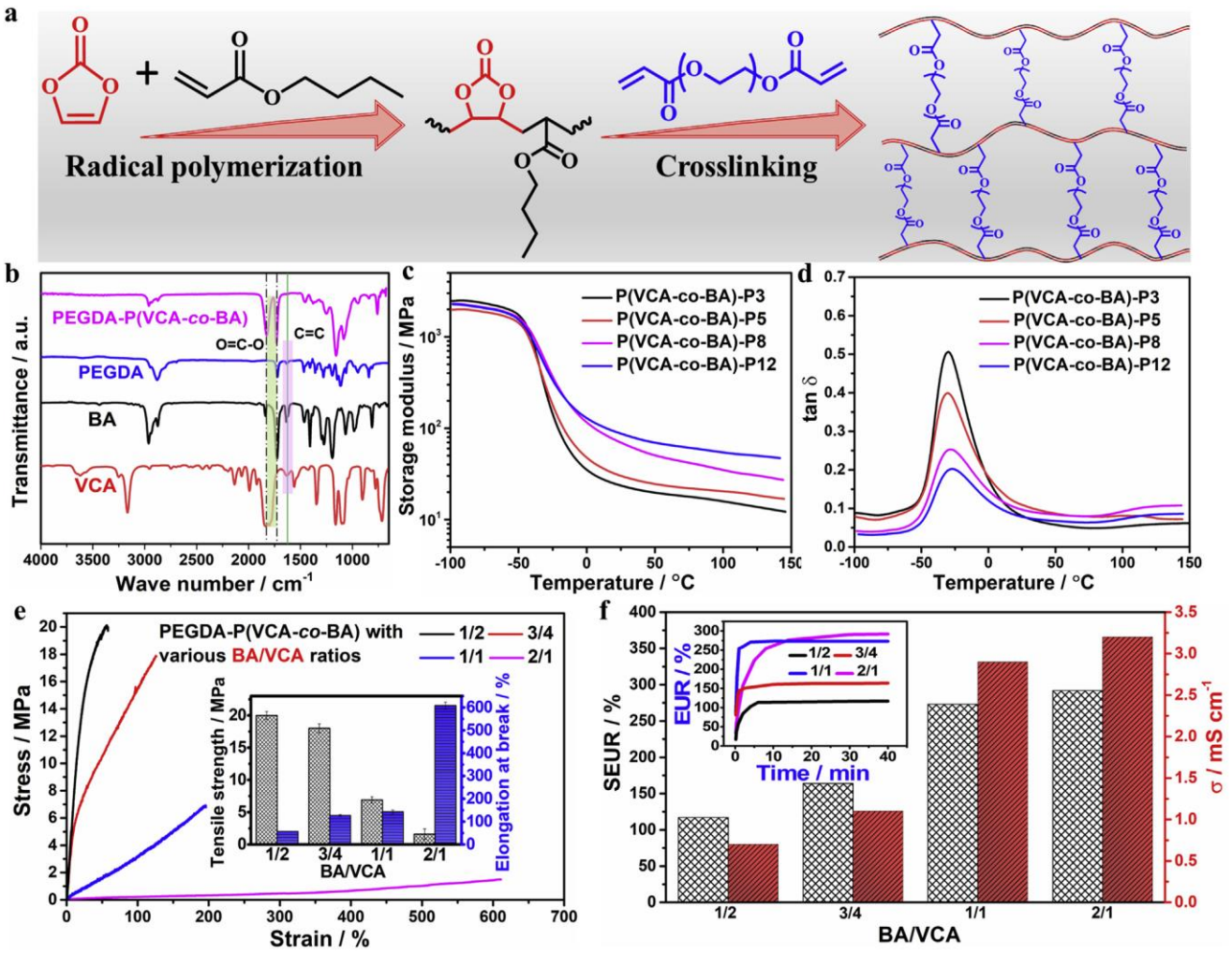

Fig. 1. (a) Synthesis route of PEGDA-P(VCA-co-BA). (b) FTIR spectra of VAC, BA, PEGDA and PEGDA-P(VCA-co-BA). (c) Storage modulus and (d) tan d of PEGDA-P(VCA-co-BA) with different PEGDA contents. (e) Stress-strain curves and (Inset) Tensile strength/elongation at break of PEGDA-P(VCA-co-BA) with various VCA/BA ratios. (f) Ionic conductivity/ saturated electrolyte uptake ratio and (Inset) Electrolyte uptake ratio -time relationship curves of PEGDA-P(VCA-co-BA) with various VCA/BA ratios.

In order to determine the optimum content of PEGDA, the effects of the PEGDA content of on the crosslinking density, mechanical properties, electrolyte uptake ratio and ionic conductivity of the products were investigated when BA:VCA was 3:4. Firstly, based on elasticity theory of rubber [**40**] and dynamic thermomechanical analysis (DMA), the crosslinking density of polymer was evaluated by storage modulus higher than Tg, and calculated by formula **Ve = E/3RT**. Where Ve is the crosslinking density, E is the storage modulus higher than Tg (usually T is Tg+40°C) and R is the ideal gas constant. The corresponding parameters were listed in **Table S3**. From **Fig. 1**c and d, it can be found that with

the increase of PEGDA content, Ve increased. When the contents of PEGDA were 8% and 12%, the crosslinking densities reached 0.0123 and 0.0144 respectively, which were an order of magnitude higher than that of 3% and 5%. In addition, **Fig. S2** showed the mechanical properties of different PEGDA contents. It was noteworthy that when the PEGDA content was 8%, the maximum tensile strength (**Fig. S2**b) reached 17.9 MPa. With the continuous addition of cross-linked agent (12%), the excess PEGDA molecules cross-linked with each other, resulting in defects in the polymer, which is manifested in the stress-strain curve, that is, the tensile strength and elongation at break decrease at the same time. Similarly, from gel content, saturated electrolyte uptake ratio (SEUR) and ionic conductivity (**Fig. S3**), as the PEGDA content increases, the gel content increases, which is beneficial to improving the solvent resistance of P(VCA-co-BA). However, the SEUR and conductivity decrease gradually. Therefore, as a compromise between mechanical properties and ionic conductivity, 8 wt% of the PEGDA mass fraction was considered to be an ideal value.

Besides the influence of cross-linked agent, the ratio of rigid segment VCA to flexible monomer BA is also directly related to whether the copolymer can be used as QPE. The effects of different monomer ratios (BA/VCA: 1/2, 3/4, 1/1, 2/1) on the properties of polymers were studied by using crosslinking agent PEGDA content of 8 wt%. From the stress-strain curves of **Fig. 1**e, it can be seen that with the increase of BA monomer, the tensile strength of the polymer decreases and the elongation at break increases. Moreover, unlike the small elongation at 1/2, 3/4 and the low tensile strength at 2/1, the difference between the tensile strength and the elongation at break is the smallest when BA/VCA ratio is 1/1. These results are attributed to the increase of BA component, which reduces the steric hindrance of single bond spin.

In addition to mechanical properties, as an electrolyte, another factor to be considered is ionic conductivity. All PEGDA-P(VCA-co-BA) copolymers with various BA/VCA ratios can reach saturation in about 10 min (**Fig. 1**f inset). As can be seen in **Fig. 1**f, with the increase of SEUR, the ionic conductivity (**s**) increases simultaneously. When the ratio of BA/VCA is 1/1, the ionic conductivity increases greatly (2.9 mS cm^{-1}), which is more than 60% higher than that of 0.7 mS cm-1 and 1.1 mS cm^{-1} with lower BA contents (1/2 and 3/4). However, when BA continues to increase to 2/1, the increase rate of ionic conductivity is significantly slowed down, which is only 9.38% (3.2 mS cm^{-1}) higher than that of 1/1. Therefore, when the ratio of BA/VCA is 1:1, the mechanical properties are not sacrificed, and the ionic conductivity can reach a higher value.

As a prerequisite parameter of electrolyte, lithium-ion transference number (t_{Li+}) is an indispensable factor to realize high power output capability and another important way to evaluate electrochemical capability of electrolyte (**Fig. 2**a and b). The relevant parameters in Bruce-Vincent-Evans formula were listed in **Table S4**. It can be found that compared with Li/LE/Li cell assembled by commercial PP sperator (0.33) [**41**], the t_{Li+} using QPE reached 0.63. High t_{Li+} is beneficial to reduce the concentration gradient on the electrode surface and achieve high power density [**42**].In order to further explain the dynamic stability between electrolyte and lithium sheet, the impedance curves (**Fig. 2**c and d) of the cells with 110 cycles under a current density of 0.1 mA cm^{-2} were tested, and the corresponding bulk resistance and interfacial resistance were compared in **Fig. 2**e and f. It was found that the resistances of LE and QPE increased significantly in the first 10 cycles, which was due to the formation of passive films on lithium electrodes during the first 10 cycles, namely the so-called "solid electrolyte interface" (SEI) [**43—45**]. In addition, it is noteworthy that the bulk resistance of Li/ LE/Li keeps floating and the interfacial resistance of Li/LE/Li is much higher than that of Li/QPE/Li, which is disadvantageous to form a stable interface with lithium. On the contrary, for Li/QPE/Li cell, both bulk resistance (Rb) and interfacial resistance (Ri) almost no longer change and tend to be stable after 10 cycles, which proves the stability interface between QPE and Li.

In addition to using carbon nanotubes as conductive skeleton to provide conductivity, nitrogen doping was introduced into the cathode, which was accomplished by electro-polymerization and calcination. The FTIR spectrum of CNT@PPy shows the characteristic peaks of PPy at 1558 and 1472 cm^{-1} corresponding to the C=C stretching and C—N stretching in the pyrrole ring, respectively, which proves that the PPy is successfully deposited onto the surface of CNT (**Fig. 3**a). **Fig. S4** are the FE-SEM images of N(PPy)-CNT at different charge levels (1.5 C, 3.6 C, 7.4 C). The nitrogen content measured by EDS and corresponding conductivity of the product were listed in **Table S5**. Considering both nitrogen content and conductivity, the optimum charge of electro-polymerization is 3.6 C.

After simple electrochemical oxidation and melting treatment, it can be seen that sulfur is uniformly distributed on the outer wall of N(PPy)-CNT (**Fig. 3**b) and the sulfur content is 62.5 wt% from TG (**Fig. S5**). By calculation, the sulfur loading in N(PPy)-CNT@S composite is as high as 4.53 mg cm^{-2}. From XRD **Fig. 3**c, it can be seen that the N(PPy)-CNT has a wide diffraction peak in the range of 20° — 30°, which corresponds to the (002) crystal plane of carbon material. In addition, the N(PPy)-CNT@S possesses two sharp peaks at 23° and 28°, and the strength of these two peaks is weaker than that of elemental sulfur, indicating that the sulfur existed mainly in low crystalline state. Similarly, in Raman results (**Fig. 3**d), the characteristic peaks of N(PPy)-CNT at 1347 and 1578 cm^{-1} correspond to the D and G bands of carbon materials, and ID/IG is 0.68. The three weak sulfur peaks of N(PPy)-CNT@S at 150, 218 and 470 cm^{-1} further prove the loading of sulfur.

The XPS spectra of N(PPy)-CNT and N(PPy)-CNT@S were shown in Fig. 3e. It is found that the N(PPy)-CNT shows the peaks corresponding to C 1s, O 1s and N 1s at 285 eV, 400 eV and 532 eV, respectively. The presence of N and O is beneficial to the adsorption of lithium polysulfide. In addition, the two peaks at 164.3 and 229 eV in N(PPy)-CNT@S belong to the binding energy of S 2p and S 2s levels, respectively. After the peak separation treatment of N 1s (**Fig. 3**f), a variety of nitrogen was found, including pyridine nitrogen (398.1 eV), pyrrolidine nitrogen (400.7 eV) and graphite nitrogen (404.1 eV).

In order to evaluate the electrochemical performances of the designed QPE, two different Li—S batteries were assembled with N(PPy)-CNT@S composite as cathode and lithium sheet as anode using PEGDA-P(VCA-co-BA)-QPE and commercial PP seperator, respectively. **Fig. 4**a shows that the cathodic peak between 2.2—2.4 V corresponds to the conversion from sulfur to higher-order Li_2S_n ($4 < n < 8$), and the cathodic peak between 1.9—2.1 V corresponds to the continuous transition to lower-order Li_2S_2/Li2S. The anodic peak represents the reversible change of discharge product Li_2S_2/Li_2S to LiPSs and eventually to S8. Compared with Li| PP|S battery, QPE has higher peak current of cathodic and anodic, which means that more substances participate in the reaction, in other words, it has stronger electrochemical reaction kinetics [**46**].

Moreover, the cathodic peak moves to the positive potential direction and the anodic peak moves to the negative potential direction, which represents a higher reversibility of redox reaction. Similarly, the charge-discharge curves at 0.1C (**Fig. 4**b) also validate this conclusion. All cells present a charge platform at -2.3 V, and two discharge platforms at -2.3 and -2.0 V, representing the typical redox reaction of sulfide oxidation and two-step sulfur reduction. In addition, it is noteworthy that the charge/discharge potential gap of Li—S batteries using QPE is only 0.13 V, which is much smaller than that of Li|PP|S batteries (0.316 V). The reduced potential gap indicates that the QPE can eliminate the effect of polysulfides accumulation by increasing ionic conductivity and absorbing dissolved polysulfides, thus significantly reducing the polarization of Li—S batteries.

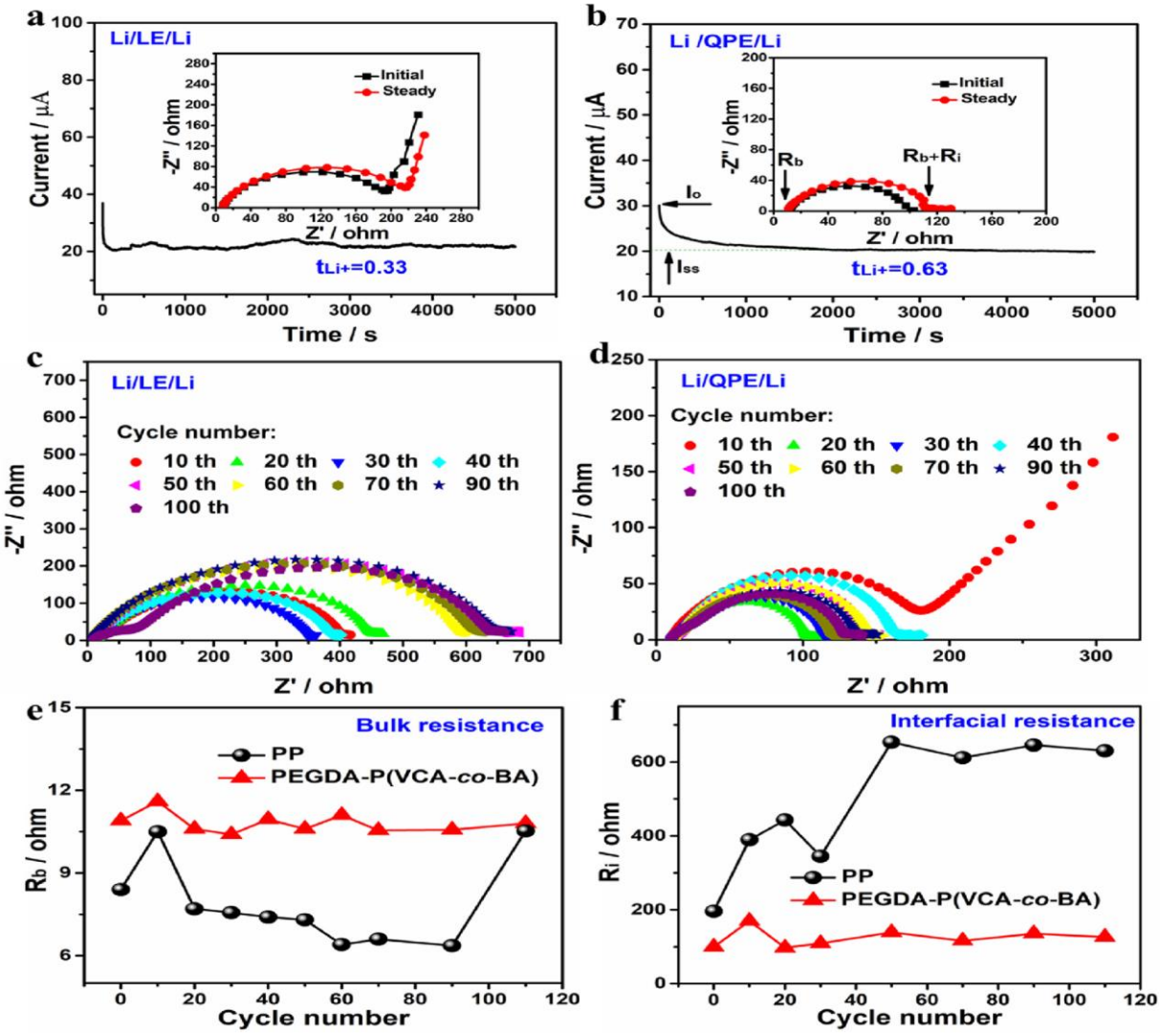

Fig. 2. (a) Polarization curves obtained by chronoamperometry for the Li/LE/Li symmetrical cell. (Inset) The corresponding impedance spectra. (b) Polarization curves obtained by chronoamperometry for the Li/PEGDA-P(VCA-co-BA)/Li symmetrical cell. (Inset) The corresponding impedance spectra. Nyquist spectra of Li electrodes of (c) Li/LE/Li and (d) Li/ PEGDA-P(VCA-co-BA)/Li with various cycles. The changes of body resistance Rb (e) and interfacial resistance Ri (f) with different cycles.

The rate performance of different cells was further tested as additional evidence for the superior electrochemical performance of QPE. As shown in **Fig. 4**c, the cells were evaluated by increasing C-rate from 0.1 C to 2 C and returning to 0.2 C. For cells using QPE, the specific capacities of 1080,947,835, 752 and 628 mA h g^{-1} at 0.1 C, 0.2 C, 0.5 C, 1C and 2 C are much higher than that of PP (999, 792, 690, 598 and 518 mA h g^{-1}). After 50 cycles, QPE exhibits a high reversible capacity of 900 mAh g^{-1} with a capacity retention rate of 95% when the rate returns to 0.2 C. These results indicate that the QPE is more effective in accelerating the rate of redox reaction in Li—S batteries because the rate capability is related to the dynamics of batteries. Fig. 4d compares the 500 cycles performance of two different cells at 0.1 C to further verify this advantage. The initial specific capacity of PP battery reaches 999 mAh g^{-1}, which is 59.6% of the theoretical value. Compared with the reported literature [**12**], the traditional S|PP|Li is only about 40% of the theoretical value.

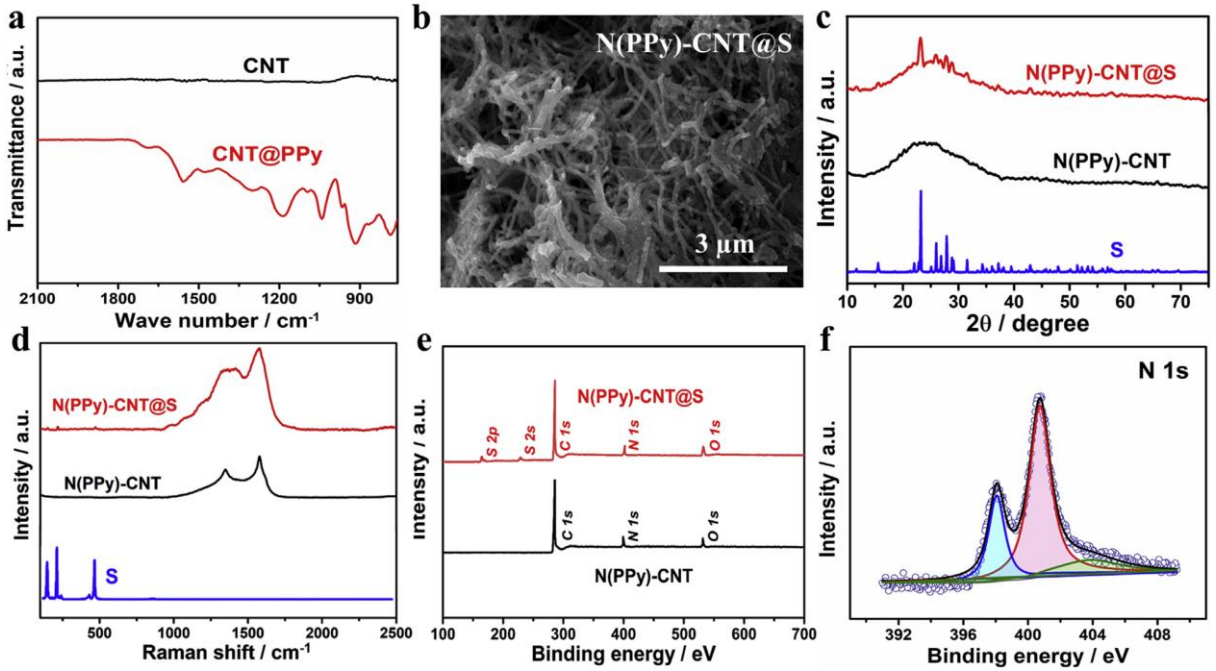

Fig. 3. (a) FTIR spectra of CNT and CNT@PPy. (b) FESEM image of N(PPy)-CNT@S. (c) XRD patterns, (d) Raman spectra of sulfur, N(PPy)-CNT, and N(PPy)-CNT@S. (e)XPS spectra with survey scan of N(PPy)-CNT and N(PPy)-CNT@S. (f) N 1s core level XPS spectra of N(PPy)-CNT@S.

It is worth noting that QPE batteries exhibit a higher initial specific capacity of 1080 mAh g^{-1} (675 mAh g^{-1} of the entire cathode) at 0.1C, reaching 64.5% of the theoretical value. The N(PPy)-CNT@S cathode's initial loading is 4.89 mAh cm^{-2} and Li anode's loading is 3.99 mAh cm^{-2} at a current density of 0.76 mA cm-2 with sulfur areal loading of 4.53 mg cm^{-2}, and the corresponding calculation parameters are listed in **Table S6**. In addition, the volumetric energy density is calculated according to the formulas [**47**]:

$$E_{v-cathode} = \rho_{-cathode} QU$$

$$E_{v-device} = f_v \, E_{v-cathode}$$

Where $E_{v\text{-cathode}}$ and $E_{v\text{-device}}$ (Wh/L) are the volumetric energy density based on cathode and device, respectively. $p_{\text{-cathode}}$ is the cathode density, g cm^{-3}; Q is the discharge capacity of the entire cathode, mAh g^{-1}; U is the discharge plateau 2.05 V; fv is the volume fraction of the cathode in the device, including anode, cathode, and QPE. The caculation shows that the $E_{v\text{-cathode}}$ reaches 1522 Wh L^{-1}, and the $E_{v\text{-device}}$ is 184 Wh L^{-1}. The lower energy density value of the device is attributed to the excess of the lithium and electrolyte. The weight ratios between electrodes and the electrolyte system are listed in **Table S7**. After 500 cycles, the capacity was maintained at 715 mAh g^{-1}, the capacity retention rate was 66.2%, and the average attenuation per cycle was only 0.068%. While the capacity of PP battery was only 248 mAh g^{-1}, and the capacity retention rate was 24.8%. The average attenuation rate per cycle is as high as 0.15%, which is 2.2 times faster than that of QPE battery. These are attributed to the co-chemical anchoring and physical barrier effects of nitrogen-doped cathode and QPE.

In order to evaluate the interfacial resistance and reversibility of Li—S batteries before and after cycling, electrochemical impedance spectroscopy (EIS) were carried out for different cells. In the Nyquist plots, the diameter of the semicircle in the middle and high frequency region corresponds to the charge transfer resistance (Rct) [**48,49**] generated by the electrochemical reaction between the electrodes and electrolytes, while the inclined line in the low frequency region is assigned to Warburg impedance (Wo), which reflects the diffusion process of polysulfides in the sulfur cathode [**50,51**]. After 500 cycles, the impedance of PP battery increases significantly compared with the initial state (**Fig. 4**e). In contrast, the impedance of QPE batteries has not changed significantly (**Fig. 4**f). Photographs of the recycled batteries are shown in the inset of **Fig. 4**e and f. It was found that the cathode and the PP seperator were separated, but closely adhered to the QPE film. Moreover, QPE film adapts to the volume deformation of the sulfur cathode during the cycling process due to its flexibility, which ensures the integrity of the cathode structure (**Fig. S6**). This further proves that the PEGDA-P(VCA-co-BA) QPE can protect the electrodes, thus forming a more stable electrode/electrolyte interface.

Compared with the irregular lithium deposition of liquid electrolyte, QPE with 3D cross-linking network benefits from its compactness to ensure the uniform deposition of lithium ions. Thus, the growth of lithium dendrites is inhibited and the contact problem between lithium anode and electrolyte is improved (**Fig. 5**a). The surface morphology changes of lithium anode before and after 500 cycles at 0.1 C were observed by FE-SEM (**Fig. S7**). Compared with fresh lithium anode and lithium anode after cycling using liquid electrolyte and QPE, it is obvious that QPE has successfully inhibited the shuttle of lithium polysulfide. In order to investigate the adsorption capacity and chemical interaction of QPE on lithium polysulfide, static adsorption experiments were carried out. As shown in **Fig. 5b**, the same size of PP seperator and PEGDA-P(VCA-co-BA) were put into 0.05 M Li_2S_6 solution. After 24 h, the color of Li2S6 solution mixed with PEGDA-P(VCA-co-BA) obviously faded, while the color of Li_2S_6 solution mixed with PP only slightly degraded. What's more, after adsorption test, PP and PEGDA-P(VCA-co-BA) were taken out and washed repeatedly. The digital photos after drying were shown in **Fig. 5**c and d. It is obvious that the adsorption of lithium polysulfide by PEGDA-P(VCA-co-BA) is a strong chemical action, so the electrolyte film turns yellow. These show that PEGDA-P(VCA-co-BA) has good capture performance and strong chemical adsorption capacity for lithium polysulfide.

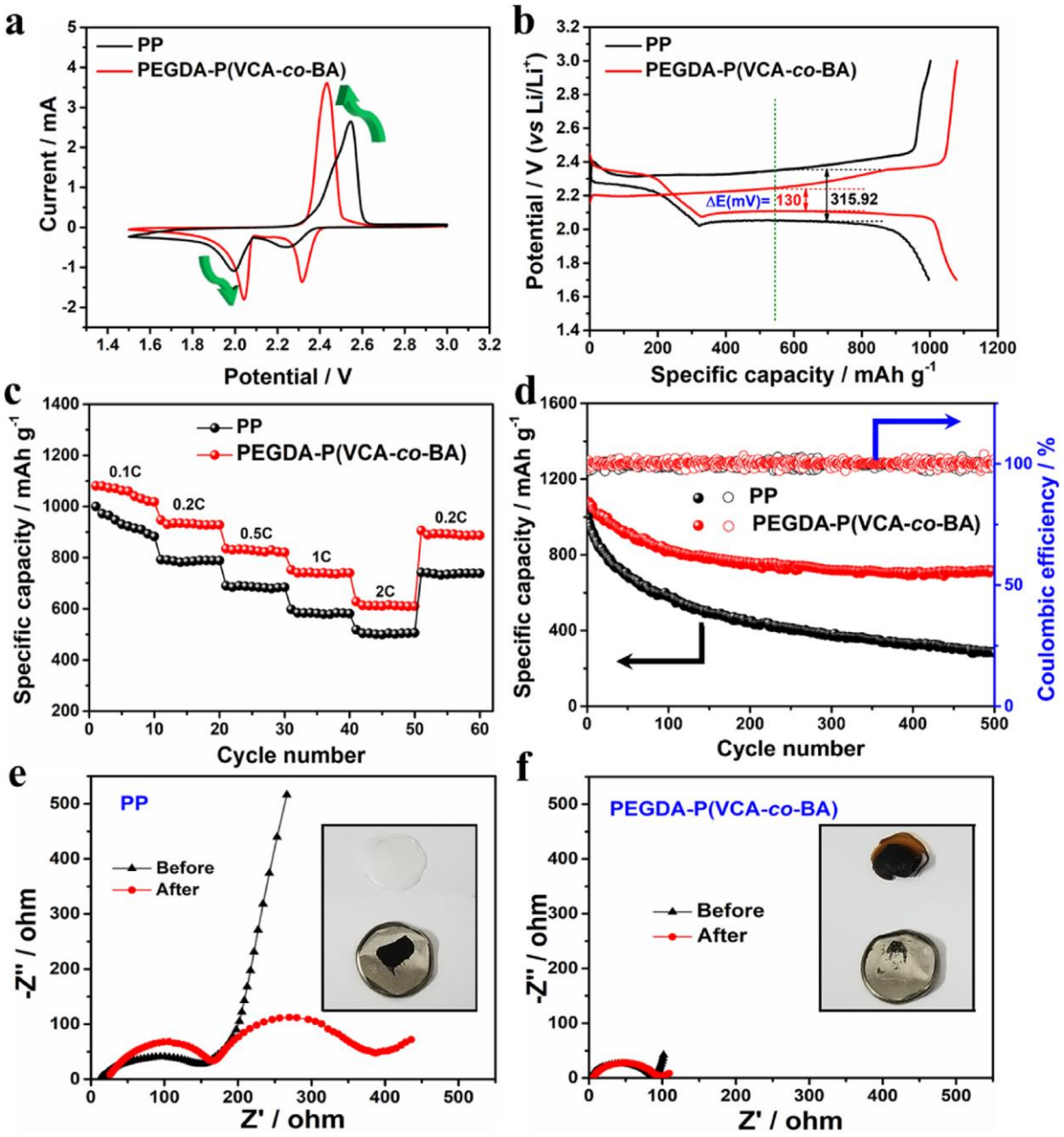

Fig. 4. (a) CV curves, (b) Charge-discharge curves, (c) Rate performance, and (d) Cyclic stability of N(Ppy)-CNT@S/PEGDA-P(VCA-co-BA)/Li cell and N(Ppy)-CNT@S/PP/Li cell. Nyquist spectra of (e) N(Ppy)-CNT@S/PP/Li before and after cycled and (f) N(Ppy)-CNT@S/PEGDA-P(VCA-co-BA)/Li. (Inset) Contact between seperator and cathode in cycled cells.

In order to further reveal the mechanism between the polysulfide and the QPE, the cycled cells were transferred to glove box, and the dismantled QPE was washed repeatedly with DOL/DME. After drying, the QPE before and after 500 cycles was characterized by XPS and ATR-FTIR. As shown in Fig. 5e, O 1s spectra are used to characterize the surface composition of QPE. It is found that the original QPE is assigned to C—O—C and C=O peaks at 531.8 eV and 530.8 eV, respectively, which are typical components of ester functional groups [**52**]. After 500 cycles, the peak of C=O in QPE disappeared completely because LiPSs were adsorbed on ester functional groups and covered the surface signals. Above results indicate that the ester groups of the PEGDA-P(VCA-co-BA) QPE play a crucial role in the chemical interaction with LiPSs. Furthermore, **Fig. 5**f compares the ATR-FTIR spectra of QPE before and after cycling. Obviously, for the carbonyl peak of VCA (ca.1825 cm^{-1}), after cycling the peak position red-shifts and the peak intensity decreases significantly. It is also found that the intensity of the

carbonyl peak in BA (ca.1725 cm^{-1}) weakens after cycling. The ATR-FTIR results also support the above viewpoints. From the crosssectional FE-SEM images of the lithium anode after cycling (**Fig. S8**), it can be seen that Li anode in QPE batteries shows a smaller corrosion depth of only 37 pm. These results further prove that the intermediate lithium polysulfide is firmly anchored on the QPE, thus slowing down the diffusion rate of polysulfide. Moreover, the introduction of ester groups with high spatial density is more conducive to the interaction with lithium polysulfide.

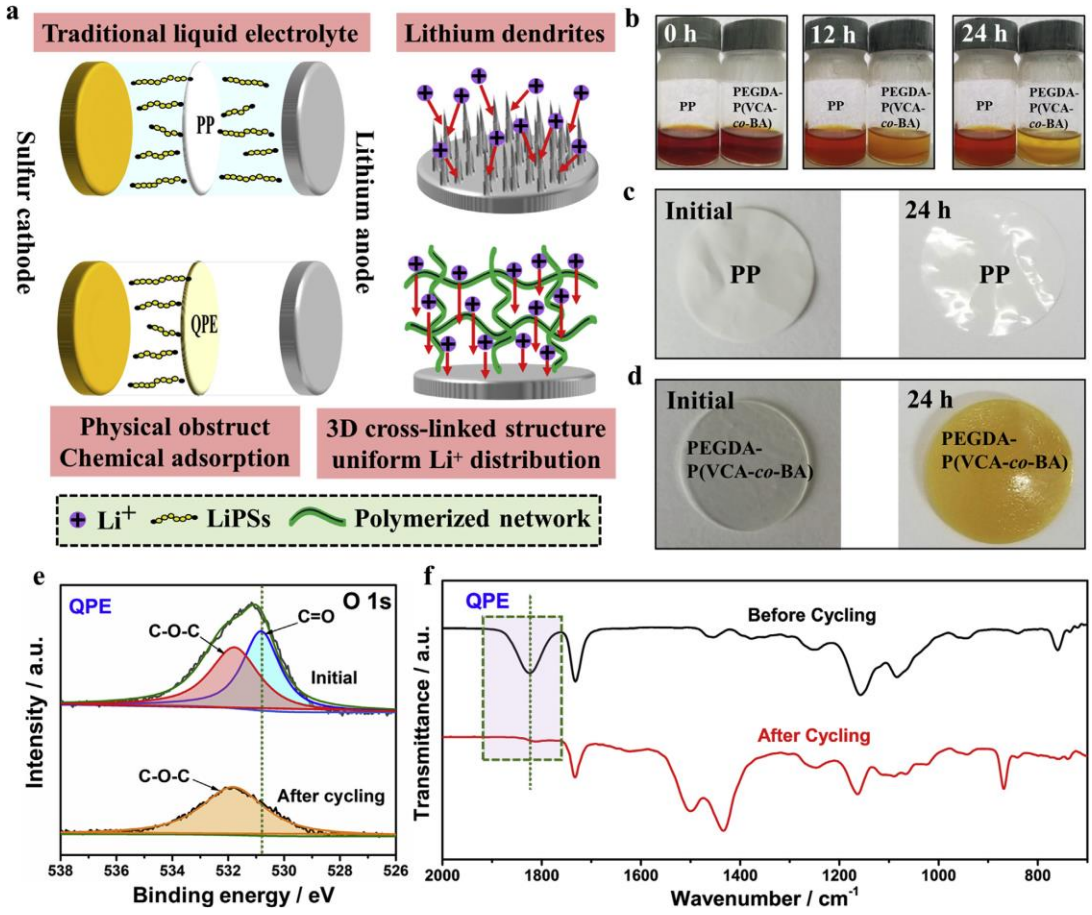

Fig. 5. (a) Schematic of QPE-based Li—S batteries for inhibiting shuttle effect. (b) Photographs of the sealed vials of a LÍ2S6/DOL/DME solution after contacting with PP and PEGDA-P(VCA-co-BA) for 24 h. Photographs of (c) PP and (d) PEGDA-P(VCA-co-BA) original form and after 24 h. (e)O1s core level XPS spectra and (f) ATR-FTIR spectra of QPE before cycling and after cycling.

4. Conclusions

In conclusion, we have successfully prepared a rigid-flexible quasi-solid-state electrolyte with three-dimensional cross-linked network structure, in which the VCA segments provide high spatial density carbonate bonds to achieve strong capture of LiPSs. On the one hand, the introduction of flexible BA segments overcomes the fragility of VCA, on the other hand, the movement of segment can effectively increase the lithium-ion transference number (t_{Li+} = 0.63). The Nyquist plots of Li//Li symmetrical batteries at different cycles show that there is a stable interface between QPE and electrodes. Therefore, the stability of lithium-sulfur batteries under long cycle was improved successfully. After 500 cycles at 0.1 C, the capacity of lithium-sulfur batteries is still 715 mAh g^{-1}, and the average attenuation is only 0.068% per cycle. Moreover, the assembled Li—S battery has good rate performance and nearly 100% Coulomb efficiency. These results indicate that the PEGDA-P(VCA-co-

BA) QPE provides an effective solution for the next generation of high-performance lithium-sulfur batteries.

References

[1] J.M. Tarascon, M. Armand, Issues and challenges facing rechargeable lithium batteries, Nature 414 (2001) 359—367.

[2] M. Armand, J.M. Tarascon, Building better batteries, Nature 451 (2008) 652—657.

[3] A. Manthiram, Y. Fu, S.H. Chung, C. Zu, Y.S. Su, Rechargeable lithium-sulfur batteries, Chem. Rev. 114 (2014) 11751 — 11787.

[4] A. Manthiram, S.H. Chung, C. Zu, Lithium-sulfur batteries: progress and prospects, Adv. Mater. 27 (2015) 1980—2006.

[5] W.S. Zhi, Y. Sun, Q. Zhang, Y. Cui, Designing high-energy lithium-sulfur batteries, Chem. Soc. Rev. 45 (2016) 5605—5634.

[6] M. Arumugam, Z.F. Yong, H.C. Sheng, X.Z. Chen, S.S. Yu, Rechargeable lithium-sulfur batteries, Che. Rev. 14 (2014) 11751 — 11787.

[7] R. Fang, S. Zhao, Z. Sun, W. Wang, H.M. Cheng, F. Li, More reliable lithium-sulfur batteries: status, solutions and prospects, Adv. Mater. 29 (2017) 1606823.

[8] W. Chen, T. Lei, C. Wu, M. Deng, C. Gong, K. Hu, Y. Ma, L. Dai, W. Lv, W. He, X. Liu, J. Xiong, C. Yan, Designing safe electrolyte systems for a high-Stability lithium-sulfur battery, Adv. Energy Mater. 8 (2018) 1702348.

[9] O. Borodin, Challenges with prediction of battery electrolyte electrochemical stability window and guiding the electrode-electrolyte stabilization, Current Opinion in Electrochemistry 13 (2019) 86—93.

[10] M. Liu, D. Zhou, Y.B. He, Y. Fu, X. Qin, C. Miao, H. Du, B. Li, Q.H. Yang, Z. Lin, T.S. Zhao, F. Kang, Novel gel polymer electrolyte for high-performance lithium-sulfur batteries, Nano Energy 22 (2016) 278—289.

[11] Q. Pang, A. Shyamsunder, B. Narayanan, C.Y. Kwok, L.A. Curtiss, L.F. Nazar, Tuning the electrolyte network structure to invoke quasi-solid state sulfur conversion and suppress lithium dendrite formation in Li-S batteries, Nat. Energy 3 (2018) 783—791.

[12] H. Qu, J. Zhang, A. Du, B. Chen, J. Chai, N. Xue, L. Wang, L. Qiao, C. Wang, X. Zang, J. Yang, X. Wang, G. Cui, Multifunctional sandwich-structured electrolyte for high-performance lithium-sulfur batteries, Adv. Sci. 5 (2018) 1700503.

[13] H. Du, S. Li, H. Qu, B. Lu, X. Wang, J. Chai, H. Zhang, J. Ma, Z. Zhang, G. Cui, Stable cycling of lithium-sulfur battery enabled by a reliable gel polymer electrolyte rich in ester groups, J. Membr. Sci. 550 (2018) 399—406.

[14] K. Park, J.H. Cho, J.-H. Jang, B.-C. Yu, A.T. De la Hoz, K.M. Miller, C.J. Ellison, J.B. Goodenough, Trapping lithium polysulfides of a Li-S battery by forming lithium bonds in a polymer matrix, Energy Environ. Sci. 8 (2015) 2389—2395.

[15] J. Chai, Z. Liu, J. Zhang, J. Sun, Z. Tian, Y. Ji, K. Tang, X. Zhou, G. Cui, A superior polymer electrolyte with rigid cyclic carbonate backbone for rechargeable lithium ion batteries, ACS Appl. Mater. Interfaces 9 (2017) 17897—17905.

[16] X. Wei, D.F. Shriver, Highly conductive polymer electrolytes containing rigid polymers, Chem. Mater. 10 (1998) 2307—2308.

[17] J. Chai, B. Chen, F. Xian, P. Wang, H. Du, J. Zhang, Z. Liu, H. Zhang, S. Dong, X. Zhou, G. Cui, Dendrite-free lithium deposition via flexible-rigid coupling composite network for LiNi0.5Mn1.5O4/Li metal batteries, Small 14 (2018) 1802244.

[18] L. Sun, H. Li, M. Zhao, G. Wang, High-performance lithium-sulfur batteries based on self-supporting graphene/carbon nanotube foam@sulfur composite cathode and quasi-solid-state polymer electrolyte, Chem. Eng. J. 332 (2018) 8—15.

[19] X. Luo, Y. Liao, H. Xie, Y. Zhu, Q. Huang, W. Li, Enhancement of cyclic stability for high voltage lithium ion battery at elevated temperature by using polyethylene-supported poly(methyl methacrylate-butyl acrylate-acrylonitrile-styrene) based novel gel electrolyte, Electrochim. Acta 220 (2016) 47—56.

[20] M. Liu, H.R. Jiang, Y.X. Ren, D. Zhou, F.Y. Kang, T.S. Zhao, In-situ fabrication of a freestanding acrylate-based hierarchical electrolyte for lithium-sulfur batteries, Electrochim. Acta 213 (2016) 871—878.

[21] J. Zhang, N. Zhao, M. Zhang, Y. Li, P.K. Chu, X. Guo, Z. Di, X. Wang, H. Li, Flexible and ion-conducting membrane electrolytes for solid-state lithium batteries: dispersion of garnet nanoparticles in insulating polyethylene oxide, Nano Energy 28 (2016) 447—454.

[22] W. Fan, N.-W. Li, X. Zhang, S. Zhao, R. Cao, Y. Yin, Y. Xing, J. Wang, Y.-G. Guo, C. Li, A dual-salt gel polymer electrolyte with 3D cross-linked polymer network for dendrite-free lithium metal batteries, Adv. Sci. 5 (2018) 1800559.

[23] X. Judez, H. Zhang, C. Li, G. Gebresilassie Eshetu, Y. Zhang, J.A. Gonzalez-Marcos, M. Armand, L.M. Rodriguez-Martinez, Polymer-rich composite electrolytes for all-solid-state Li-S cells, J. Phys. Chem. Lett. 8 (2017) 3473—3477.

[24] Y. Yang, G. Zheng, Y. Cui, Nanostructured sulfur cathodes, Chem. Soc. Rev. 42 (2013) 3018—3032.

[25] L. Ma, K. Hendrickson, S. Wei, L. Archer, Nanomaterials: Science and applications in the lithium-sulfur battery, Nano Today 10 (2015) 315—338.

[26] G. Zhou, L. Li, C. Ma, S. Wang, Y. Shi, N. Koratkar, W. Ren, F. Li, H.-M. Cheng, A graphene foam electrode with high sulfur loading for flexible and high energy Li-S batteries, Nano Energy 11 (2015) 356—365.

[27] J. Zhang, C.-P. Yang, Y.-X. Yin, L.-J. Wan, Y.-G. Guo, Sulfur encapsulated in graphitic carbon nanocages for high-rate and long-cycle lithium-sulfur batteries, Adv. Mater. 28 (2016) 9539—9544.

[28] Q. Pang, C.Y. Kwok, D. Kundu, X. Liang, L.F. Nazar, Lightweight metallic MgB2 mediates polysulfide redox and promises high-energy-density lithium-sulfur batteries, Joule 3 (2019) 136—148.

[29] X. Ye, J. Ma, Y.-S. Hu, H. Wei, F. Ye, MWCNT porous microspheres with an efficient 3D conductive network for high performance lithium-sulfur batteries, J. Mater. Chem. 4 (2016) 775—780.

[30] G. Li, W. Lei, D. Luo, Y. Deng, Z. Deng, D. Wang, A. Yu, Z. Chen, Stringed "tube on cube'' nanohybrids as compact cathode matrix for high-loading and lean-electrolyte lithium-sulfur batteries, Energy Environ. Sci. 11 (2018) 2372—2381.

[31] G. Hu, Z. Sun, C. Shi, R. Fang, J. Chen, P. Hou, C. Liu, H.-M. Cheng, F. Li, A sulfur-rich copolymer@CNT hybrid cathode with dual-confinement of polysulfides for high-performance lithium-sulfur batteries, Adv. Mater. 29 (2017) 1603835.

[32] P. Strubel, S. Thieme, T. Biemelt, A. Helmer, M. Oschatz, J. Brueckner, H. Althues, S. Kaskel, ZnO hard templating for synthesis ofhierarchical porous carbons with tailored porosity and high performance in lithium-sulfur battery, Adv. Funct. Mater. 25 (2015) 287—297.

[33] C. Hu, C. Kirk, Q. Cai, C. Cuadrado-Collados, J. Silvestre-Albero, F. Rodriguez-Reinoso, M.J. Biggs, A High-volumetric-capacity cathode based on interconnected close-packed N-doped porous carbon nanospheres for long-life lithium-sulfur batteries, Adv. Energy Mater. 7 (2017) 1701082.

[34] J. Guo, X. Du, X. Zhang, F. Zhang, J. Liu, Facile formation of a solid electrolyte interface as a smart blocking layer for high-stability sulfur cathode, Adv. Mater. 29 (2017) 1700273.

[35] H.J. Peng, G. Zhang, X. Chen, Z.-W. Zhang, W.-T. Xu, J.-Q. Huang, Q. Zhang, Enhanced electrochemical kinetics on conductive polar mediators for lithium-sulfur batteries, Angew. Chem. Int. Ed. 55 (2016) 12990—12995.

[36] Q. Li, Y. Song, R. Xu, L. Zhang, J. Gao, Z. Xia, Z. Tian, N. Wei, M.H. Rummeli, X. Zou, J. Sun, Z. Liu, Biotemplating growth of nepenthes-like N-doped graphene as a bifunctional polysulfide scavenger for Li-S batteries, ACS Nano 12 (2018) 10240—10250.

[37] J. Song, T. Xu, M.L. Gordin, P. Zhu, D. Lv, Y.B. Jiang, Y. Chen, Y. Duan, D. Wang, Nitrogen-doped mesoporous carbon promoted chemical adsorption of sulfur and fabrication of high-areal-capacity sulfur cathode with exceptional cycling stability for lithium-sulfur batteries, Adv. Funct. Mater. 24 (2014) 1243—1250.

[38] Z. Sun, J. Zhang, L. Yin, G. Hu, R. Fang, H.-M. Cheng, F. Li, Conductive porous vanadium nitride/graphene composite as chemical anchor of polysulfides for lithium-sulfur batteries, Nat. Commun. 8 (2017) 14627.

[39] G.B. Appetecchi, G. Dautzenberg, B. Scrosati, A new class of advanced polymer electrolytes and their relevance in plastic-like, rechargeable lithium batteries, J. Electrochem. Soc. 143 (1996) 6—12.

[40] S.F. Edwards, Dynamical theory of rubber elasticity, Polym. J. 17 (1985) 271—276.

[41] M. Riley, P.S. Fedkiw, S.A. Khan, Transport properties of lithium hectorite-based composite electrolytes, J. Electrochem. Soc. 149 (2002) A667—A674.

[42] K. Ito, N. Nishina, H. Ohno, High lithium ionic conductivity of poly (ethylene oxide) s havingsulfonate groups on their chain ends, J. Mater. Chem. 7 (1997) 1357—1362.

[43] J. Yue, M. Yan, Y.-X. Yin, Y.-G. Guo, Progress of the interface design in all-solid-state Li-S batteries, Adv. Funct. Mater. 15 (2018) 282—290.

[44] D. Zheng, X.Q. Yang, D. Qu, The stability of the solid electrolyte interface on the Li electrode in Li-S batteries, ACS Appl. Mater. Interfaces 8 (2016) 10360—10366.

[45] Y. Lu, X. Huang, Z. Song, K. Rui, Q. Wang, S. Gu, J. Yang, T. Xiu, M.E. Badding, Z. Wen, Highly stable garnet solid electrolyte based Li-S battery with modified anodic and cathodic interfaces, Energy Storage Materials 28 (2018) 282—290, 28.

[46] J. He, G. Hartmann, M. Lee, G.S. Hwang, Y. Chen, A. Manthiram, Freestanding 1T MoS2/graphene heterostructures as a highly efficient electrocatalyst for lithium polysulfides in Li-S batteries, Energy Environ. Sci. 12 (2019) 344—350.

[47] H. Li, F.Y. Kang, H.Q. Yang, Dense graphene monolith for high volumetric energy density Li-S batteries, Adv. Funct. Mater. 8 (2018) 1703438.

[48] J. Hassoun, B. Scrosati, Moving to a solid-state configuration: a valid approach to making lithium-sulfur batteries viable for practical applications, Adv. Mater. 22 (2010) 5198—5201.

[49] K. Xu, Electrolytes and interphases in Li-ion batteries and beyond, Chem. Rev. 114 (2014) 11503—11618.

[50] M. Wang, H. Zhang, W. Zhou, X. Yang, X. Li, H. Zhang, Rational design of a nested pore structure sulfur host for fast Li/S batteries with a long cycle life, J. Mater. Chem. 4 (2015) 1653—1662.

[51] J. Xu, D. Su, W. Zhang, W. Bao, G. Wang, A nitrogen-sulfur co-doped porous graphene matrix as a sulfur immobilizer for high performance lithium-sulfur batteries, J. Mater. Chem. 4 (2016) 17381 — 17393.

[52] E. Yilmaz, H. Sezen, S. Suzer, Probing the charge build-up and dissipation on thin PMMA film surfaces at the molecular level by XPS, Angew. Chem. Int. Ed. 51 (2012) 5488—5492.